Natural Compounds as Inhibitors of SARS-CoV-2 Main Protease (3CL^{pro}): A Molecular Docking and Simulation Approach to Combat COVID-19

Md Tabish Rehman[1*], Mohamed F. AlAjmi[1], Afzal Hussain[1]

[1]Department of Pharmacognosy, College of Pharmacy, King Saud University, Riyadh-11451, Kingdom of Saudi Arabia

Running title: Natural compound-based inhibitors against COVID-19.

***Corresponding author:**

Dr. Md Tabish Rehman, Ph.D.

Department of Pharmacognosy
College of Pharmacy
King Saud University
Riyadh-11451
Kingdom of Saudi Arabia
E-mail: mrehman@ksu.edu.sa

ABSTRACT

Recently, the emergence and dissemination of SARS-CoV-2 has caused high mortality and enormous economic loss. In the fight against COVID-19, the rapid development of new drug molecules is the need of hour. However, the conventional approaches of drug development is time consuming and expensive in nature. In this study, we have adopted an alternative approach to identify lead molecules from natural sources using high throughput virtual screening approach. Ligands from natural compounds library from Selleck Inc (L1400) have been screened to evaluate their ability to bind and inhibit the main protease (M^{pro} or $3CL^{pro}$) of SARS-CoV-2, which is a potential drug target. We found that Kaempferol, Quercetin, and Rutin were able to bind at the substrate binding pocket of $3CL^{pro}$ with high affinity (10^5-10^6 M^{-1}) and interact with the active site residues such as His41 and Cys145 through hydrogen bonding and hydrophobic interactions. In fact, the binding affinity of Rutin was much higher than Chloroquine (1000 times) and Hydroxychloroquine (100 times) and was comparable to that of the reference drug Remdesivir, which is in clinical trials to treat COVID-19 patients. The results suggest that natural compounds such as flavonoids have the potential to be developed as novel inhibitors of SARS-CoV-2 with a comparable potency as that of Remdesivir. However, their clinical usage on COVID-19 patients is a subject of further investigations and clinical trials.

Keywords: SARS-CoV-2, COVID-19, Autodock, Schrodinger, Docking, Natural compounds, Flavonoids.

1. INTRODUCTION

The world is facing a threatening public health crisis and economic burden due to the emergence and spread of a novel coronavirus (nCoV). The first case of nCoV with pneumonia-like symptoms was reported in the Huanan seafood market, Wuhan, Hubei, China on Dec 12, 2019[1–3]. The Chinese authorizes ruled out the possibility of influenza and other coronaviruses on the basis of laboratory testing. However, later on Jan 7, 2020, Chinese authorities have officially announced the isolation of a new type of coronavirus and published its genome sequence[4]. On Jan 22, 2020, nCoV has been declared to be originated from wild bats and belonged to Group 2 of beta-coronavirus that also contains Severe Acute Respiratory Syndrome-Coronavirus (SARS-CoV). Although, nCoV and SARS-CoV belong to the same beta coronavirus subgroup, the similarity at genome level is only 70%. Also, nCoV has been found to show genetic differences from SARS-CoV[5]. The international Committee on Taxonomy of Viruses renamed nCoV as SARS-CoV-2. According to World Health Organization (WHO), SARS-CoV-2 spreads faster than its two ancestors SARS-CoV and Middle East Respiratory Syndrome-Coronavirus (MERS-CoV), but has a lower fatality rate of 2-3%. On Mar 11, 2020, WHO declared SARS-CoV-2 as a pandemic infectious disease of international concern. Till May 23, 2020, there have been 5,105,881 confirmed cases of coronavirus disease 2019 (COVID-2019) with 333,446 confirmed deaths.

An analysis of the SARS-CoV-2 genome revealed that it is 29.9 kb long containing 11 open reading frames (ORFs) (https://www.ncbi.nlm.nih.gov/genome/86693). Two-thirds of SARS-CoV-2 genome encodes viral polymerase (RdRp), RNA synthesis materials, and two large non-structural polypeptides (ORF1a-ORF1b). The remaining one-third of the genome encodes four structural proteins namely spike (S), envelope (E), membrane (M), nucleocapsid (N), and other accessory proteins[6]. ORF1a encodes pp1a polypeptide which contains among other protein, two viral proteases namely papain-like protease (PL^{pro}) and 3C-like protease ($3CL^{pro}$), also known as the main protease (M^{pro}). These proteases further cleave polypeptides pp1a and pp1ab (encoded by ORF1b) into 16 functional non-structural proteins (nsps). These nsps play essential roles in the activation of the viral replication process. Some of these nsps are single stranded RNA binding protein (nsp9), growth factor-like protein (nsp10), viral RNA-dependent RNA polymerase (nsp12), RNA helicase (nsp13), exo-ribonuclease (nsp14), endo-ribonuclease (nsp15) and 2´-O-ribose methyl-transferase (nsp16). Previously, it has been shown that the main protease (i.e. $3CL^{pro}$) of SARS-CoV is indispensible for the initiation of

viral life cycle, while the spike protein (S) interacts with the angiotensin converting enzyme 2 (ACE2) of the receptor cells to gain an entry into it [Luan et al., 2020]. The first X-ray crystal structure of the main protease (i.e. $3CL^{pro}$) of SARS-CoV-2 was reported by Jin et al. (2020)[7]. The structure was refined to a resolution of 2.16 Å in complex with a peptide-like inhibitor (N3). The $3CL^{pro}$ structure is composed of 306 amino acid residues which get folded into three characteristics domains. Domain I (residues 8-101) and domain II (residues 102-184) adopt an antiparallel β-barrel structure. Domain III (residues 201-300) is composed of five α-helices and is connected to domain II through a connecting loop (residues 185-200). The substrate binding site is well conserved among the coronaviruses and is located in the cleft between domains I and II, and it harbours His41-Cys145 catalytic dyad. The structural features of SARS-CoV-2 are similar to that reported for SARS-CoV[8,9]. The peptide-like inhibitor N3 binds at the substrate binding pocket in an extended conformation in such a way that the backbone of N3 formed an antiparallel sheet with residues 164-168 on one strand, and with residues 189-191 of the loop joining domains II and III. It formed a covalent bond with one of the catalytic residues Cys145, while other residues involved in the interactions were Thr24, Thr25, His41, Met49, Tyr54, Phe140, Leu141, Asn142, His163, Met165, Glu166, Leu167, Pro168, His172, Phe185, Asp187, Gln189, and Gln192 along with two water molecules[7]. These residues constitute the substrate binding site of $3CL^{pro}$.

Despite the enormous efforts by scientists all over the world, a potential drug to treat COVID-19 is yet to be announced. However, some promising leads have been identified such as Remdesivir, Ivermectin, Chroloquine, Hydroxychloroquine, Favipiravir, Azithromycin, Tocilizumab, Lopinavir/Ritonavir + Ribavirin, etc [www.clinicaltrials.gov]. Thus, there is a pressing need to identify and develop novel drugs against SARS-CoV-2. However, conventional methods of drug development is time consuming and costly in nature. The emergence of computational-aided drug discovery based on receptor structure has proved that it can help to identify potential drug-like lead molecules in a short time, and thereby assist the pharmaceutical companies to develop them into potential drug candidates.

In this study, we have screened the ability of natural compounds (L1400 library, available at www.selleckchem.com) to bind and inhibit the main protein (M^{pro} or $3CL^{pro}$) of SARS-CoV-2 using AutoDock4.2. The stability of protein-inhibitor complex was evaluated by performing molecular dynamics simulation using Desmond (Schrodinger-2018, LLC, NY, USA). The results were compared with some reference drugs having potential anti-SARS-CoV-2 activity.

2. RESULTS

2.1. Inhibition of 3CL^{pro} with the reference drugs

The relative binding positions of reference drugs such as Chloroquine, Hydroxychloroquine, Remdesivir and Ivermectin on 3CLpro is represented in **supplementary Figure S1**. All of them were found to bind at the substrate binding site of 3CL^{pro} and interact with several key amino acid residues (**supplementary Figure S2**).

2.1.1. Chloroquine-3CL^{pro} interaction

The binding energy and binding affinity of Chloroquine towards 3CL^{pro} were estimated to be -5.2 kcal/mol and 6.5 × 10^3 M^{-1} respectively (**Table 1**). It formed one hydrogen bond (Glu166) and two hydrophobic interactions (His41 and Met165) with 3CL^{pro}. Some other residues forming van der Waals interactions with Chloroquine were Tyr54, Cys145, His164, Pro168, Asp187, Arg188, Gln189, Thr190, and Gln192 (**supplementary Figure 2A, Table 2**).

2.1.2. Hydroxychloroquine-3CL^{pro} interaction

The binding energy and binding affinity of Hydroxychloroquine towards 3CL^{pro} were estimated to be -5.7 kcal/mol and 1.5 × 10^4 M^{-1} respectively (**Table 1**). It formed two hydrogen bonds (Phe140 and Glu166) and two hydrophobic interactions (alkyl and Pi-alkyl) with Met165 of 3CL^{pro}. Some other residues forming van der Waals interactions with Hydroxychloroquine were His41, Leu141, Asn142, Gly143, Ser144, Cys145, His163, His164, Asp187, Arg188, Gln189, Thr190, and Gln192 (**supplementary Figure 2B, Table 2**).

2.1.3. Remdesivir-3CL^{pro} interaction

The binding energy and binding affinity of Remdesivir towards 3CL^{pro} were estimated to be -7.5 kcal/mol and 3.2 × 10^5 M^{-1} respectively (**Table 1**). It formed six hydrogen bonds (two with Gly143, and one each with Thr24, His164, Glu166 and Gln189) and two hydrophobic interactions (His41 and Met49) with 3CL^{pro}. Some other residues forming van der Waals interactions with Remdesivir were Thr25, Thr26, Cys44, Thr45, Ser46, Tyr54, Phe140, Asn142, Ser144, Cys145, Met165, Asp187, and Arg188 (**supplementary Figure 2C, Table 2**).

2.1.4. Ivermectin-3CL^{pro} interaction

The binding energy and binding affinity of Ivermectin towards 3CL^{pro} were estimated to be -9.3 kcal/mol and 6.6 × 10^6 M^{-1} respectively (**Table 1**). It formed two hydrogen bonds (Tyr239 and Leu287) and three hydrophobic interactions (Val171, Ala194 and Leu272) with 3CL^{pro}.

Some other residues forming van der Waals interactions with Ivermectin were Asp127, Asn133, Lys137, Thr169, Gly195, Thr199, Lys236, Tyr237, Asn238, and Leu286 (**supplementary Figure 2D, Table 2**).

Table 1: Molecular docking of reference drugs with the main protease of SARS-nCoV-2 (3CL^{pro})

S. No.	Drugs	PubChem ID	Structure of drug molecule	Docking energy (kcal/mol)
1.	Chloroquine	2719	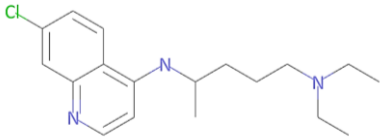	-5.2
2.	Hydroxychloroquine	3652	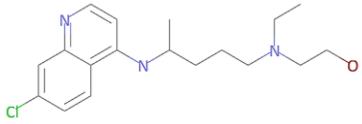	-5.7
3.	Remdesivir	121304016	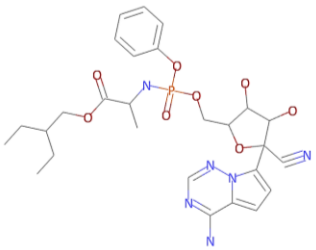	-7.5
4.	Ivermectin	6321424	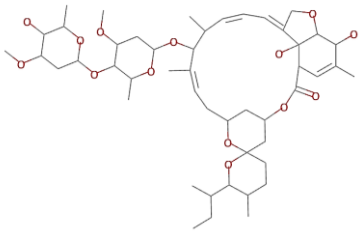	-9.3

Table 2: The interaction and molecular forces between reference drugs and the main protease of SARS-CoV-2 ($3CL^{pro}$)

Donor -atom	Acceptor-atom	Distance (Å)	Type of interaction
Chloroquine			
UNK:H	GLU166:O	2.2278	Conventional Hydrogen
HIS41	UNK	5.6833	Hydrophobic (Pi-Pi T-shaped)
UNK	MET165	4.6266	Hydrophobic (Pi-Alkyl
Hydroxychloroquine			
UNK:H	PHE140:O	2.3534	Conventional Hydrogen Bond
UNK:H	GLU166:OE2	2.2705	Conventional Hydrogen Bond
UNK:Cl	MET165	4.4506	Hydrophobic (Alkyl)
UNK	MET165	4.4597	Hydrophobic (Pi-Alkyl)
Remdesivir			
GLY143:HN	UNK:N	2.5027	Conventional Hydrogen Bond
GLY143:HN	UNK:O	1.8477	Conventional Hydrogen Bond
GLU166:HN	UNK:O	2.5248	Conventional Hydrogen Bond
UNK:HN	THR24:O	2.5595	Conventional Hydrogen Bond
UNK:P	HIS164:O	3.5894	Conventional Hydrogen Bond
UNK:H	GLN189:OE1	2.2841	Conventional Hydrogen Bond
MET49:SD	UNK	4.8529	Pi-Sulfur bond
HIS41	UNK	3.8607	Hydrophobic (Pi-Pi Stacked)
MET49	UNK	5.4812	Hydrophobic (Alkyl)
Ivermectin			
TYR239:HH	UNK:O	2.0622	Conventional Hydrogen Bond
LEU287:HN	UNK:O	2.0446	Conventional Hydrogen Bond
ALA194	UNK:C	4.1552	Hydrophobic (Alkyl)
UNK:C	LEU272	5.1807	Hydrophobic (Alkyl)
UNK:C	VAL171	3.9125	Hydrophobic (Alkyl)

2.2. Inhibition of $3CL^{pro}$ with natural compounds

Virtual screening of natural compounds revealed that their docking energies varied in -9.4 to -2.0 kcal/mol range. The high affinity compounds having a docking score of ≤ -7.5 kcal/mol were shortlisted for further analysis by binding pose examination (**Table 3**). We found that only Kaempferol, Quercetin and Rutin were able to bind at the substrate binding site of $3CL^{pro}$ with high affinity. However, the binding sites of other high affinity compounds such as Bicornin, Biflorin, Ellagic acid, Maslinic acid and Oleanolic acid has been located distinct to the substrate binding site (**supplementary Figure S1**). Hence, the interaction of Bicornin, Biflorin, Ellagic acid, Maslinic acid and Oleanolic acid with $3CL^{pro}$ has been discussed in the supplementary data (**supplementary Figure S3, Table S1**).

Table 3: Molecular docking of the most potent natural compounds (≤ -7.5 kcal/mol) towards the main protease of SARS-nCoV-2 (3CL^{pro})

S. No.	Compounds	PubChem ID	Structure of compound	Docking energy (kcal/mol)
1.	Bicornin	71308161	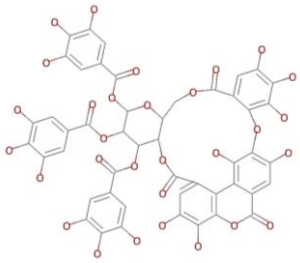	-9.2
2.	Biflorin	441959	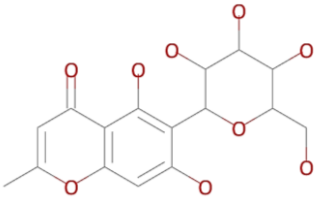	-8.5
3.	Ellagic acid	5281855	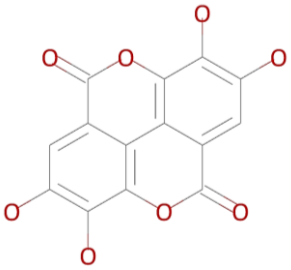	-8.4
4.	Kaempferol	5280863	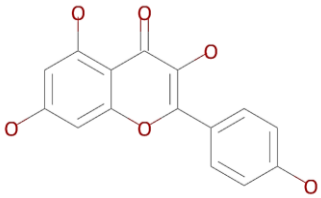	-7.8
5.	Maslinic acid	73659		-8.1
6.	Oleanolic acid	10494		-8.5

7.	Quercetin	5280343	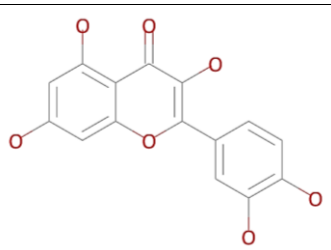	-7.5
8.	Rutin	5280805	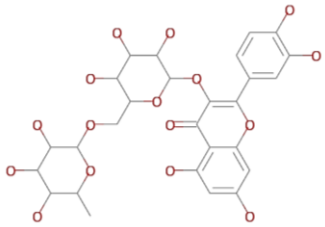	-9.4

2.2.1. Kaempferol-3CL^{pro} interaction

The binding energy and binding affinity of Kaempferol towards 3CL^{pro} were estimated to be -7.8 kcal/mol and 5.2 × 10^5 M^{-1} respectively (**Table 3**). It formed two hydrogen bonds (Leu141 and Gln189), one Pi-donor hydrogen bond with Glu166, three Pi-sulfur bonds (two with Cys145 and one with Met165) and two hydrophobic interactions (Met49 and His41) with 3CL^{pro}. Some other residues forming van der Waals interactions with Kaempferol were Tyr54, Phe140, Asn142, Ser144, His163, His164, Asp187 and Arg188 (**Figure 1, Table 4**).

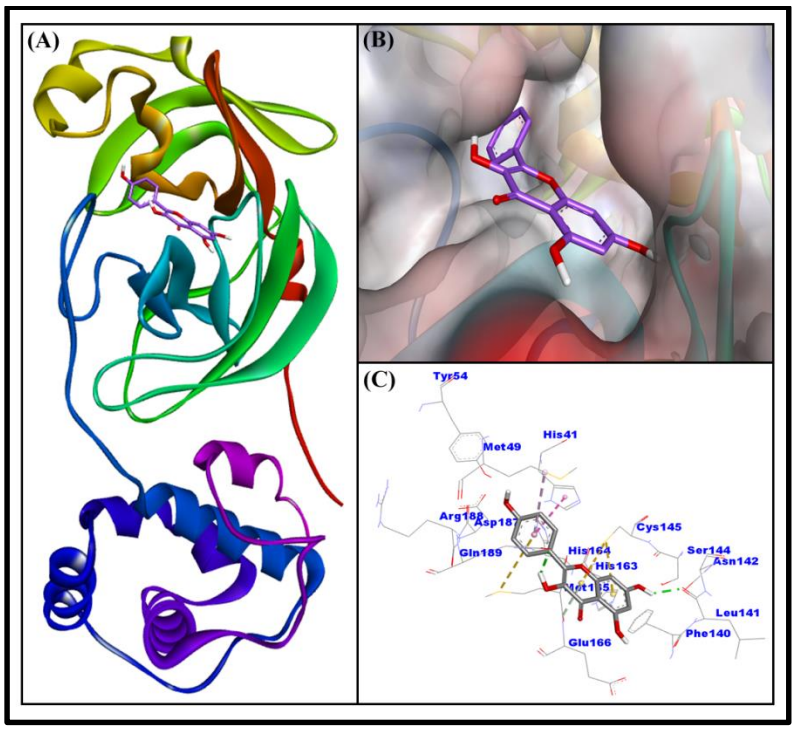

Figure 1: Molecular docking of Kaempferol with 3CL^{pro} of SARS-CoV-2. Binding of Kaempferol to 3CL^{pro} catalytic site, represented in (A) Two-dimension, and (B) Three-dimension. (C) Interaction of Kaempferol with key amino acid residues of 3CL^{pro}.

2.2.2. Quercetin-3CL^{pro} interaction

The binding energy and binding affinity of Quercetin towards 3CL^{pro} were estimated to be -7.5 kcal/mol and 3.2 × 10^5 M^{-1} respectively (**Table 3**). It formed three hydrogen bonds (Ser144, His163 and Gln189), one Pi-donor hydrogen bond with Glu166, and two hydrophobic interactions (Met49 and Met165) with 3CL^{pro}. Some other residues forming van der Waals interactions with Quercetin were His41, Tyr54, Phe140, Leu141, His164, Asp187 and Arg188 (**Figure 2, Table 4**).

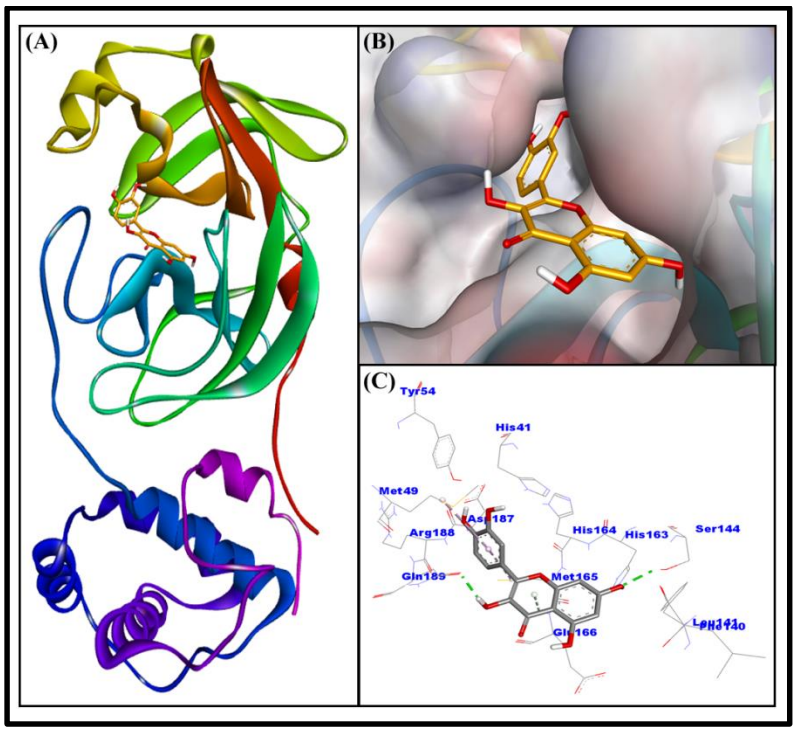

Figure 2: Molecular docking of Quercetin with 3CL^{pro} of SARS-CoV-2. Binding of Quercetin to 3CL^{pro} catalytic site, represented in (A) Two-dimension, and (B) Three-dimension. (C) Interaction of Quercetin with key amino acid residues of 3CL^{pro}.

2.2.3. Rutin-3CL^{pro} interaction

The binding energy and binding affinity of Rutin towards 3CL^{pro} were estimated to be -9.4 kcal/mol and 7.8 × 10^6 M^{-1} respectively (**Table 3**). It formed eight hydrogen bonds (two each with Thr26, Gly143, His163, and one each with Asn142 and Ser144), one Pi-sulfur bond with Cys145, and two hydrophobic interactions with Met49 of 3CL^{pro}. Some other residues forming van der Waals interactions with Rutin were Leu27, His41, Tyr54, Phe140, Leu141, His164, Met165, Glu166, Asp187, Arg188 and Gln189 (**Figure 3, Table 4**).

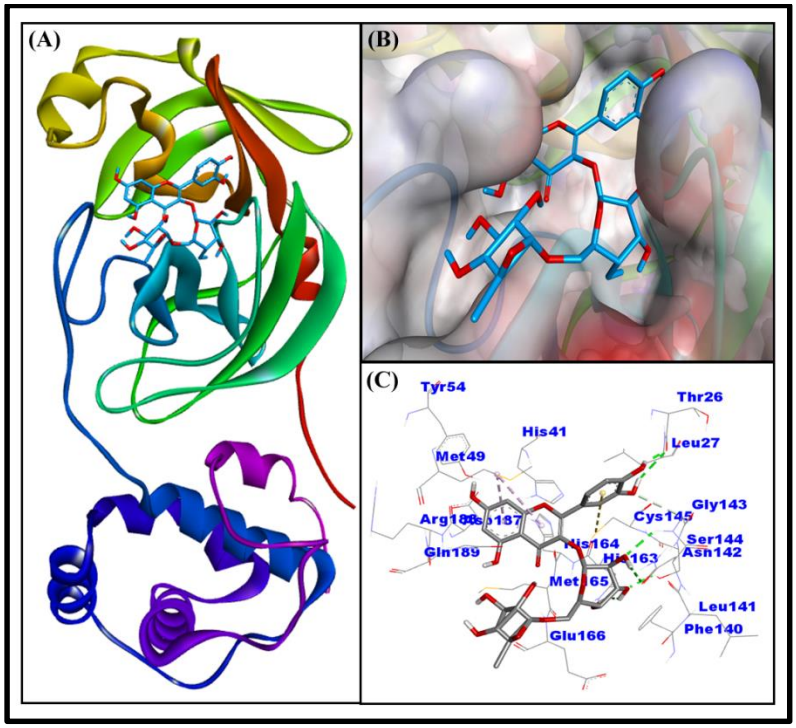

Figure 3: Molecular docking of Rutin with 3CL^{pro} of SARS-CoV-2. Binding of Rutin to 3CL^{pro} catalytic site, represented in (A) Two-dimension, and (B) Three-dimension. (C) Interaction of Rutin with key amino acid residues of 3CL^{pro}.

Table 4: The interaction and molecular forces between the natural compounds and the main protease of SARS-CoV-2 (3CL^{pro})

Donor -atom	Acceptor-atom	Distance (Å)	Type of interaction
Kaempherol			
UNK:H	GLN189:OE1	2.1235	Conventional Hydrogen Bond
UNK:H	LEU141:O	2.0703	Conventional Hydrogen Bond
GLU166:HN	UNK	3.0410	Pi-Donor Hydrogen Bond
CYS145:SG	UNK	5.6364	Pi-Sulfur Bond
CYS145:SG	UNK	5.0215	Pi-Sulfur Bond
MET165:SD	UNK	5.3727	Pi-Sulfur Bond
HIS41	UNK	4.8458	Hydrophobic (Pi-Pi Stacked)
UNK	MET49	4.7871	Hydrophobic (Pi-Alkyl)
Quercetin			
SER144:HG	UNK:O	2.2136	Conventional Hydrogen Bond
UNK1:H	GLN189:OE1	2.0500	Conventional Hydrogen Bond
UNK1:H	HIS163:NE2	2.1245	Conventional Hydrogen Bond
GLU166:HN	UNK	2.8827	Pi-Donor Hydrogen Bond
UNK	MET49	5.1959	Hydrophobic (Pi-Alkyl)
UNK	MET165	5.0533	Hydrophobic (Pi-Alkyl)
Rutin			
GLY143:HN	UNK:O	2.4035	Conventional Hydrogen Bond
SER144:HG	UNK:O	2.1205	Conventional Hydrogen Bond

UNK:H	THR26:O	2.5633	Conventional Hydrogen Bond
UNK:H	THR26:O	1.9755	Conventional Hydrogen Bond
UNK:H	ASN142:OD1	2.5782	Conventional Hydrogen Bond
UNK:H	HIS163:NE2	2.3939	Conventional Hydrogen Bond
UNK:H	HIS163:NE2	2.2541	Conventional Hydrogen Bond
GLY143:CA	UNK:O	3.4214	Carbon Hydrogen Bond
CYS145:SG	UNK	5.1309	Pi-Sulfur Bond
UNK	MET49	4.7295	Hydrophobic (Pi-Alkyl)
UNK	MET49	4.2636	Hydrophobic (Pi-Alkyl)

2.3. Molecular dynamics simulation of $3CL^{pro}$ with natural compounds

2.3.1. Root mean square deviations (RMSDs) estimation

As compared to the initial frame, root mean square deviations (RMSDs) in the backbone of $3CL^{pro}$ alone or in complex with different ligands as a function of simulation time are presented in **Figure 4A**. It was noticed that for the first 400-600 ps, large fluctuation in RMSD values (up to 3.1 Å) of protein alone were observed due to the equilibration of initial protein structure. Consequently, a steady-state dynamics was then maintained throughout the simulation time and the RMSD values varied with in the acceptable limit of 2 Å. Similarly, the RMSD values of $3CL^{pro}$ with bound ligand (Kaempferol, Quercetin and Rutin) were within the upper limit of 2 Å, after an initial fluctuation for 500-600 ns. A small variation in RMSD values during the start of simulation was due to the entry of a large ligand into the binding site cavity. Subsequently, establishment of complementary contacts between protein and ligands led to the formation of a stable protein-ligand complex, as indicated by steadied RMSD values.

2.3.2. Root mean square fluctuations (RMSFs) determination

Moreover, the root mean square fluctuations (RMSFs) along the $3CL^{pro}$ side chains were measured to monitor any conformational changes associated with the binding of Kaempferol, Quercetin and Rutin (**Figure 4B**). A large RMSF values were observed at the N- and C-terminal ends of the protein, as they tend to fluctuate more due to their unbound positions. For the middle part of the protein, it was observed that all the fluctuations in 3CLpro side chain overlaps with the B-factor which was measured experimentally during X-ray crystallography. The results of RMSDs and RMSFs confirmed the formation of a stable protein-ligand complex.

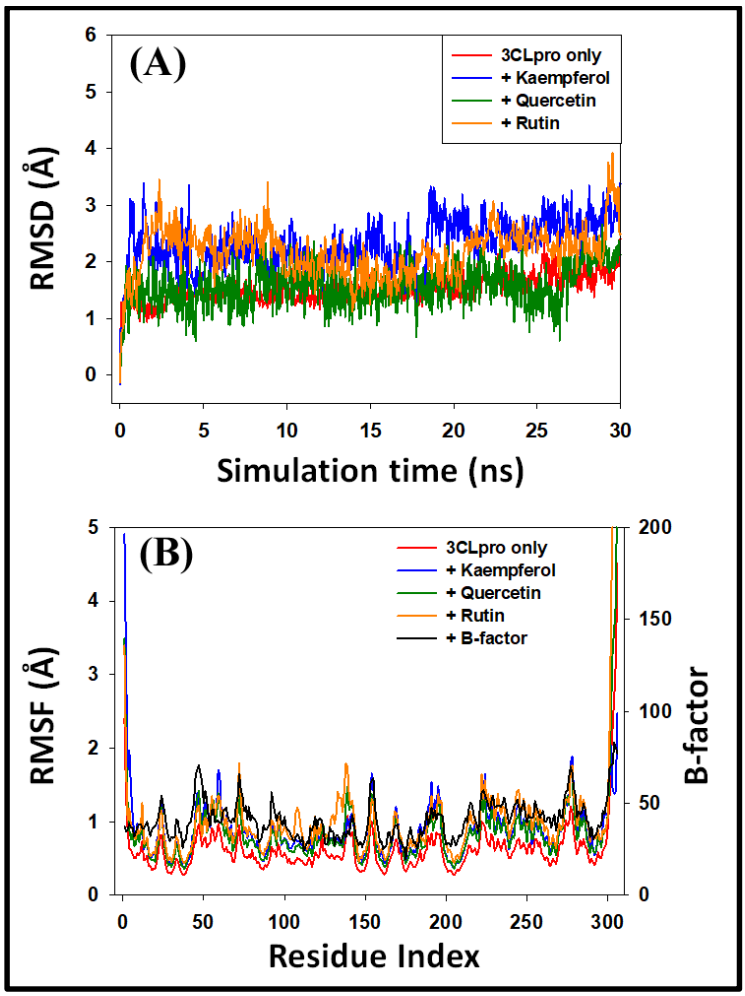

Figure 4: Molecular dynamics simulation of 3CL^{pro} in the presence of different ligands. Variations in (A) Root mean square deviation (RMSD), and (B) Root mean square fluctuation (RMSF) values as a function of simulation time.

2.3.3. Interaction pattern and secondary structure prediction

During the course of simulation, ligands (Kaempferol, Quercetin and Rutin) made several interactions with 3CL^{pro} (**Figures 5-7**). Kaempferol formed hydrogen bonds, hydrophobic interactions and water bridges with some crucial amino acid residues of 3CL^{pro} such as His41 and Gln189 throughout the simulation time (**Figure 5A,C**). Some other residues of the substrate binding site were also involved in 3CL^{pro}-Kaempferol complex formation such as Thr25, Thr26, Cys44, Thr45, Ser46, Met49, Tyr54, Asn119, Asn142, Cys145, His164, Met165, Glu166, Val186, Asp187, Arg188, Thr190, Ala191 and Gln192. The total numbers of contacts formed between Kampferol and 3CL^{pro} during simulation were in the range of 2-10 (**Figure 5C**). Similarly, Quercetin formed hydrogen bonds, hydrophobic interactions and water bridges with some crucial amino acid residues of 3CL^{pro} such as His41, Met49, Glu166, Asp187, Thr190 and Gln192 throughout the simulation time (**Figure 6A,C**). Some other

residues of the substrate binding site were also involved in 3CL^{pro}-Quercetin complex formation such as Thr25, Cys44, Thr45, Ser46, Asp48, Tyr54, Asn142, Cys145, His164, Met165, Leu167, Pro168, Thr169, Val186, Arg188, and Gln189. The total numbers of contacts formed between Quercetin and 3CL^{pro} during simulation were in the range of 2-12 (**Figure 6C**). Furthermore, Rutin formed hydrogen bonds, hydrophobic interactions and water bridges with crucial amino acid residues of 3CL^{pro} such as Thr26, Gly143, Ser144, Cys145 Met165, Pro168, Gln189, Thr190 and Gln192 throughout the simulation time (**Figure 7A,C**). Some other residues of the substrate binding site were also involved in 3CL^{pro}-Rutin complex formation such as Thr24,Thr25, His41, Cys44, Thr45, Ser46, Glu47, Met49, Asn119, Phe140, Leu141, Asn142, His163, His164, Glu166, Leu167, Thr169, Val186, Asp187, Ala191 Phe305 and Gln306. The total numbers of contacts formed between Kampferol and 3CL^{pro} during simulation were in the range of 7-17 (**Figure 7C**).

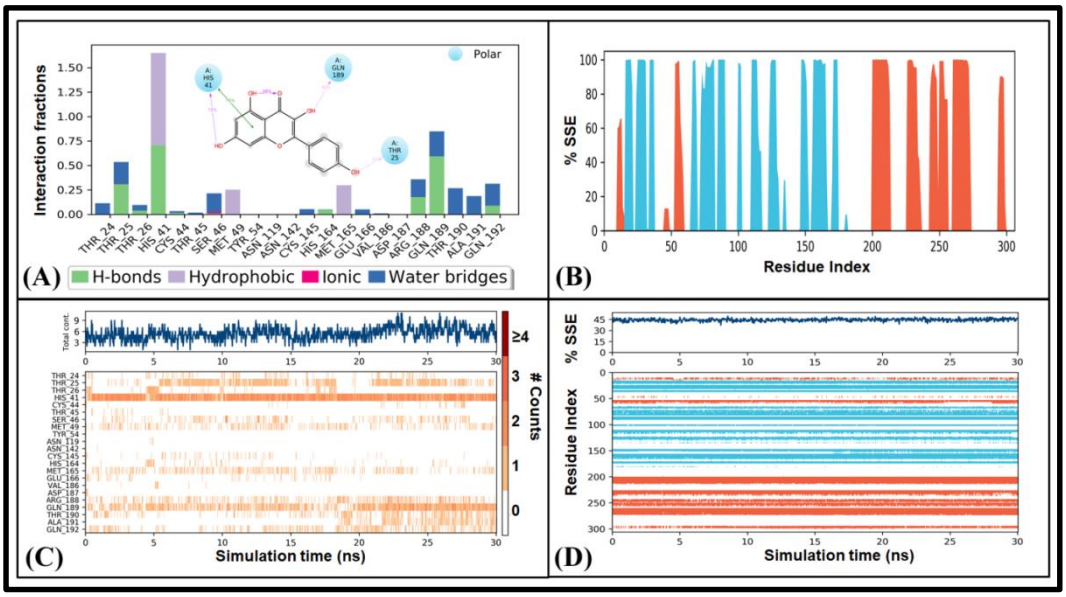

Figure 5: Panels (A) and (C) represent 3CL^{pro}-Kaempferol contacts formed during simulation. Panels (B) and (D) represent secondary structure of protein during the course of simulation. Plots in (B) and (D) coloured in Brown and Blue demonstrate α-helices and β-strands respectively.

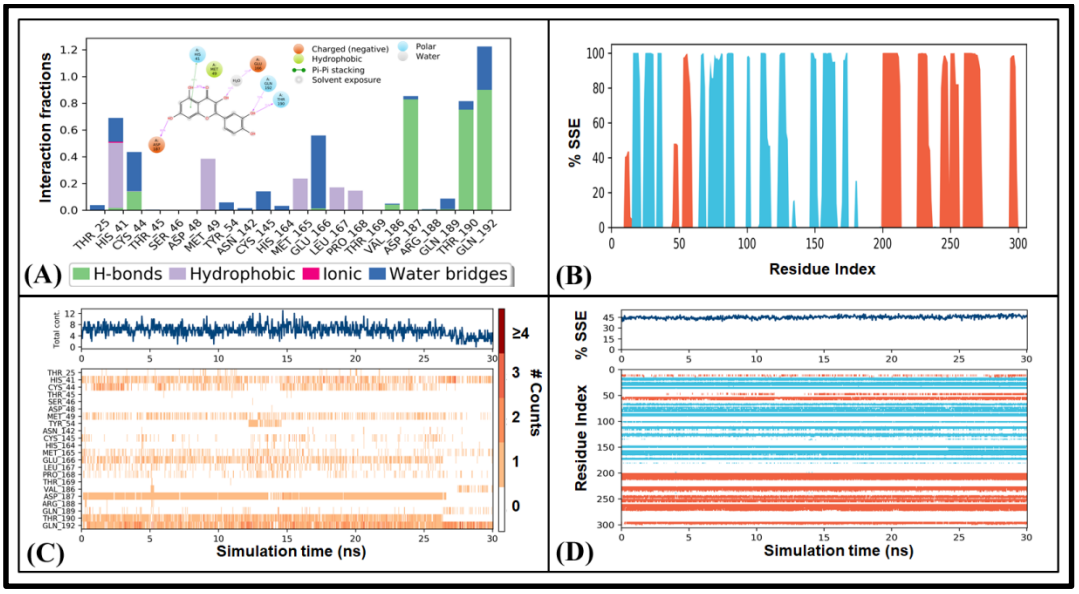

Figure 6: Panels (A) and (C) represent 3CL^{pro}-Quercetin contacts formed during simulation. Panels (B) and (D) represent secondary structure of protein during the course of simulation. Plots in (B) and (D) coloured in Brown and Blue demonstrate α-helices and β-strands respectively.

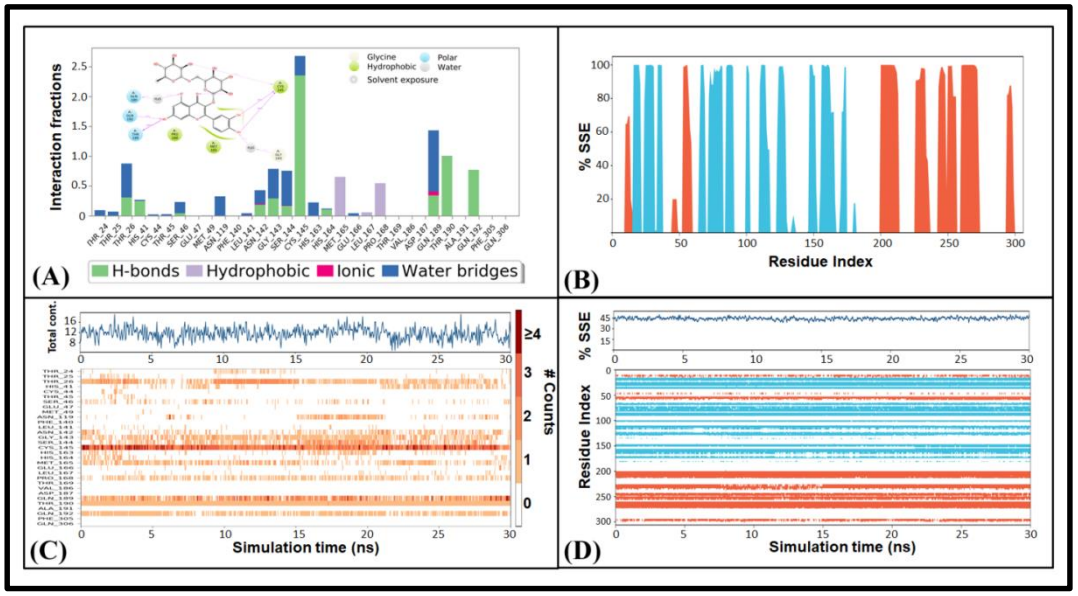

Figure 7: Panels (A) and (C) represent 3CL^{pro}-Rutin contacts formed during simulation. Panels (B) and (D) represent secondary structure of protein during the course of simulation. Plots in (B) and (D) coloured in Brown and Blue demonstrate α-helices and β-strands respectively.

The variation in the secondary structure of 3CL^{pro} upon ligand binding during the course of simulation was also monitored (**Figures 5-7**). The contribution of individual amino acid residues in maintaining the structure of 3CLpro upon binding of Kaempferol, Quercetin and

Rutin is presented in **Figures 5B**, **6B** and 7B respectively. During the course of simulation time, variations in the percentage secondary structural element (SSE) and contribution of each amino acid residues in preserving the structure of $3CL^{pro}$ due to Kaempferol, Quercetin and Rutin binding is represented in **Figures 5D**, **6D** and **7D** respectively. From the analysis of above results, it is evident that the secondary structure of $3CL^{pro}$ remains stable as a result of ligand binding.

2.3.4. Determination radius of gyration (rGyr) and surface areas

The rGyr of Kaempferol, Quercetin and Rutin was also determined as a function of simulation time (**Figure 8A**). The rGyr values for Kaempferol, Quercetin and Rutin were observed to vary within limits around 3.63 Å, 3.73 Å and 3.82 Å respectively. Further, molecular surface area (MolSA), solvent accessible surface area (SASA) and polar surface area (PSA) of Kaempferol, Quercetin and Rutin were determined during the course of simulation (**Figures 8B-D**). The values of MolSA, SASA and PSA of Kaempferol were estimated to be around 247.2 Å, 120.1 Å and 242.6 Å respectively. Similarly, MolSA, SASA and PSA of Quercetin were found to vary within limits around 257.4 Å, 102.5 Å and 279.3 Å repectively, while the values of MolSA, SASA and PSA of Rutin were within limits around 259.8 Å, 154.5 Å and 307.4 Å respectively. It is clear from the results of rGyr, MolSA, SASA and PSA that the values were varied within the acceptable limits throughout the simulation time, suggesting a stable conformation.

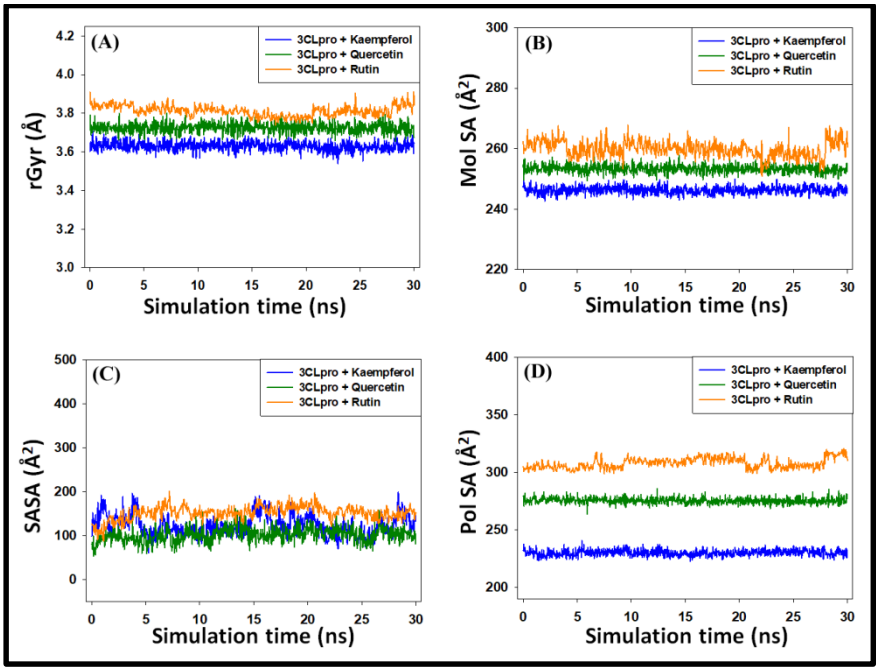

Figure 8: Dependence of (A) Radius of gyration (rGyr), (B) Molecular surface area (MolSA), (C) Solvent accessible surface area (SASA), and (D) Polar surface area (PSA) as a function of simulation time.

3. DISCUSSION

In the last two decade, the emergence of infectious agents such as SARS-CoV, MERS-CoV and SARS-CoV-2 have caused epidemics with high mortality and enormous economic loss. In the fight against such infectious agents, the rapid development of new drug molecules is needed. However, the conventional approaches of drug development is time consuming and costly in nature. In this study, we explored the use of computational approach in screening a library of natural compounds (L1400 from Selleck Inc containing 2230 compounds) for their affinity towards the main protease of SARS-CoV-2 ($3CL^{pro}$). Some reports suggest the potential of a few drugs such as Chloroquine, Hydroxychloroquine, Remdesivir, Ivermectin etc in treating COVID-19 patients. However, the mechanisms of action of these drugs are still unknown. We have included these molecules as reference drugs to delineate their mechanisms of action and for the comparative analysis of interaction between natural compounds and $3CL^{pro}$.

An analysis of the binding between reference drugs and $3CL^{pro}$ revealed that Chloroquine, Hydroxychloroquine and Remdesivir were bound at the substrate binding site and interact with the key residues of $3CL^{pro}$ (**supplementary Figure 1A**). However, the binding site of Ivermectin was located in domain III and the interconnecting loop (**supplementary Figure 1A**). The above results clearly indicate that both Remdesivir and Ivermectin were good binder of SARS-CoV-2 main protease ($3CL^{pro}$). Our results are in agreement with earlier report that Remdesivir binds at the substrate binding pocket of SARS-CoV-2[10]. Although, the binding affinity of Ivermectin was 10-folds higher than that of Remdesivir, it does not fit into the substrate binding site of $3CL^{pro}$. Hence, Remdesivir appears to be a better drug for the treatment of COVID-19 as it binds the substrate site of $3CL^{pro}$ with high affinity.

The virtual screening of natural compounds towards $3CL^{pro}$ has shown that the binding energy was in the range of -2.0 to -9.4 kcal/mol. The natural compounds having a binding energy of $\leq$ -7.5 kcal/mol were considered as a potential inhibitor of $3CL^{pro}$ and hence further analysed (**Table 3**). Molecular docking analysis revealed that the shortlisted natural compounds bind at three different sites at $3CL^{pro}$ (**supplementary Figure 1B**). Rutin, Quercetin and Kaempferol were found to bind at the substrate binding site of $3CL^{pro}$, similar to cognate N3 ligand (the peptide-like inhibitor of $3CL^{pro}$), located at the interface of domains I and II. They were found to be the most potential natural compounds that may inhibit the activity of $3CL^{pro}$, as they interact with both the catalytic residues (His41 and Cys145). Flavonoids are a significant

group of plant-derived natural products having a polyphenolic structure. They are best known for their anti-oxidant, anti-inflammatory, anti-carcinogenic properties and have been widely used in the treatment of cancer, Alzheimer's, atherosclerosis, etc[11–17]. The dietary sources of Kaempferol include Apples, grapes, tomatoes, green tea, potatoes, onions, broccoli, Brussels sprouts, squash, cucumbers, lettuce, green beans, peaches, blackberries, raspberries, spinach, etc[18–20]. Similarly, the dietary sources of Quercetin are vegetables, fruits and beverages, spices, soups, fruit juices[21–24]; and Rutin are Green tea, grape seeds, red pepper, apple, citrus fruits, berries, peaches, etc[25–27].

Although, some other natural compounds like Bicornin, Biflorin, Ellagic acid, Maslinic acid and Oleanolic acid have high binding affinities, they do not interact with $3CL^{pro}$ at the substrate binding site. They were found to bind $3CL^{pro}$ at the interface of domain III and a loop connecting domain III to domain II (**supplementary Figure 1B**). This binding site is similar to the binding site of Ivermectin. Further, Ellagic acid was found to bind at the back of the substrate binding site (**supplementary Figure 1B**).

Molecular dynamics simulation is a widely used computational technique to evaluate the stability and dynamics of a protein-ligand complex. The initial structures of $3CL^{pro}$-ligand (Kaempferol, Quercetin and Rutin) complexes were subjected to molecular dynamics simulation for 30 ns. The analysis of RMSD, RMSF, rGyr, and solvent accessibility results revealed the formation of a stable protein-ligand complex. Further, the overall secondary structure of $3CL^{pro}$ remained conserved throughout the simulation time, indicating a stable protein-ligand complex.

4. CONCLUSION

The global challenge in the form of COVID-19 outbreak has motivated us to discover, design and repurpose the already known and well-characterized natural compounds as potential inhibitors of SARS-CoV-2. Here, we have screened a natural compound library (L1400) to identify potential inhibitors of the main protease of SARS-CoV-2 i.e. $3CL^{pro}$ using molecular docking and molecular dynamics simulation. We found that Kaempferol, Quercetin, and Rutin were bound at the substrate binding site of $3CL^{pro}$ with high affinity. In fact, the binding affinity of Rutin was much higher than Chloroquine and Hydroxychloroquine and was comparable to that of the reference drug Remdesivir. Further, we have shown that Remdesivir which is in clinical trial acts by binding and inhibiting the main protease i.e. $3CL^{pro}$ of SARS-

CoV-2. The findings of this study may be useful to develop more potent and specific inhibitors of SARS-CoV-2. However, the compounds mentioned in this study need further experimental validation for their safe usage in COVID-19 patients.

5. MATERIAL AND METHODS

5.1. Retrieval and preparation of ligands/reference drugs

The natural compounds library of Selleck Inc. (Catalog No. L1400) were retrieved from www.selleckchem.com. It contains 2230 compounds in sdf format, curated from natural sources. This library represents a collection of structurally diverse, bioactive and cell permeable compounds, suitable for high throughput screening. On the basis of literature, some reference drugs such as Chloroquine, Hydroxychloroquine, Remdesivir and Ivermectin were also included in the study for the comparative analysis of binding. The two-dimensional structural information in sdf format of all the reference drugs was downloaded from PubChem database (https://pubchem.ncbi.nlm.nih.gov/). Prior to molecular docking, all the ligands were prepared by adding hydrogen atoms and merging them with non-polar hydrogen atoms. Gasteiger partial charges were added, rotatable bonds were defined, and the energies were minimized using MMFF94 forcefield[28,29].

5.2. Retrieval and preparation of protein target

The three-dimensional coordinates of the main protease (M^{pro}), also known as 3C-like protein ($3CL^{pro}$), was downloaded from the protein databank available at https://www.rcsb.org/structure/6LU7. The structure was solved to a resolution of 2.16 Å and is bound with a peptide-like inhibitor (N3)[7]. The structure of target was prepared for molecular docking by adding hydrogen atoms, Kollman united atom type charges and solvation parameters using AutoDock Tool (ADT)[30]. The whole protein molecule was considered as a potential binding site for the ligands and hence an affinity grid map of 51×67×59 Å dimensions placed at -26×12×59 Å with 0.375 Å spacing was generated using AutoGrid. Other AutoDock parameters were set to their default values and distance-depended dielectric functions were employed to calculate van der Waals and electrostatic parameters[31,32].

5.3. Molecular docking and simulation

The molecular docking between target protein and ligands was performed in Autodock4.2 using Lamarack genetic algorithm (LGA), and Solis and Wets local search methods, as

described previously[30,33]. The initial position, torsion and orientation of ligands were set randomly, and all the torsions were relaxed during docking. A total of 10 docking runs were performed and each was run was set to terminate after 2,500,000 energy calculations. The population size, translational step, and quaternion and torsion steps were set to their default values of 150, 0.2 Å and 5 respectively. The best pose of the ligand bound to target protein was selected for further analysis using Discovery Studio2.5 (Accelrys).

The molecular dynamics simulation was performed to evaluate the stability of protein-ligand complex. Desmond (Schrodinger-2018, LLC, NY, USA) was employed to perform a simulation of 30 ns under NPT (298 K and 1.013 bars) conditions, as described previously[34–36]. Briefly, the protein-ligand complex was placed in an orthorhombic simulation box, and solvated with TIP3P explicit water molecules. The boundaries of the system were at least 10 Å away from the surface of protein-ligand complex. The system was neutralized by adding proper number of counterions (Na^+ or Cl^-), and the physiological osmotic conditions were maintained by providing 150 mM NaCl. Before subjecting to molecular dynamics simulation, the energy of the system was minimized with 2000 iteration with 1 kcal/mol/Å convergence criteria. Temperature and pressure were maintained using Nose-Hoover Chain thermostat and Martyna-Tobias-Klein barostat respectively[37,38]. During simulation, a time step of 2 fs was fixed and the energies and structures were recorded every 10 ps. Post simulation analysis was performed Simulation Interaction Diagram module (Schrodinger-2018, LLC, NY, USA) and the graphs were plotted with the help of Sigma Plot 10.

Conflict of interest

Authors declare no conflict of interests.

Acknowledgement

Authors acknowledge the generous support from the Deanship of Scientific Research at King Saud University, Riyadh, Saudi Arabia, for funding this research group under grant No. RGP-1441-150.

REFERENCES

(1) Zhu, N.; Zhang, D.; Wang, W.; Li, X.; Yang, B.; Song, J.; Zhao, X.; Huang, B.; Shi, W.; Lu, R.; Niu, P.; Zhan, F.; Ma, X.; Wang, D.; Xu, W.; Wu, G.; Gao, G. F.; Tan, W. A Novel Coronavirus from Patients with Pneumonia in China, 2019. *N. Engl. J. Med.* **2020**, *382* (8). https://doi.org/10.1056/NEJMoa2001017.

(2) Li, Q.; Guan, X.; Wu, P.; Wang, X.; Zhou, L.; Tong, Y.; Ren, R.; Leung, K. S. M.; Lau, E. H. Y.; Wong, J. Y.; Xing, X.; Xiang, N.; Wu, Y.; Li, C.; Chen, Q.; Li, D.; Liu, T.; Zhao, J.; Liu, M.; Tu, W.; Chen, C.; Jin, L.; Yang, R.; Wang, Q.; Zhou, S.; Wang, R.; Liu, H.; Luo, Y.; Liu, Y.; Shao, G.; Li, H.; Tao, Z.; Yang, Y.; Deng, Z.; Liu, B.; Ma, Z.; Zhang, Y.; Shi, G.; Lam, T. T. Y.; Wu, J. T.; Gao, G. F.; Cowling, B. J.; Yang, B.; Leung, G. M.; Feng, Z. Early Transmission Dynamics in Wuhan, China, of Novel Coronavirus-Infected Pneumonia. *New England Journal of Medicine*. 2020. https://doi.org/10.1056/NEJMoa2001316.

(3) Zhou, P.; Yang, X. Lou; Wang, X. G.; Hu, B.; Zhang, L.; Zhang, W.; Si, H. R.; Zhu, Y.; Li, B.; Huang, C. L.; Chen, H. D.; Chen, J.; Luo, Y.; Guo, H.; Jiang, R. Di; Liu, M. Q.; Chen, Y.; Shen, X. R.; Wang, X.; Zheng, X. S.; Zhao, K.; Chen, Q. J.; Deng, F.; Liu, L. L.; Yan, B.; Zhan, F. X.; Wang, Y. Y.; Xiao, G. F.; Shi, Z. L. A Pneumonia Outbreak Associated with a New Coronavirus of Probable Bat Origin. *Nature* **2020**, *579* (7798). https://doi.org/10.1038/s41586-020-2012-7.

(4) Wu, F.; Zhao, S.; Yu, B.; Chen, Y. M.; Wang, W.; Song, Z. G.; Hu, Y.; Tao, Z. W.; Tian, J. H.; Pei, Y. Y.; Yuan, M. L.; Zhang, Y. L.; Dai, F. H.; Liu, Y.; Wang, Q. M.; Zheng, J. J.; Xu, L.; Holmes, E. C.; Zhang, Y. Z. A New Coronavirus Associated with Human Respiratory Disease in China. *Nature* **2020**, *579* (7798). https://doi.org/10.1038/s41586-020-2008-3.

(5) Gralinski, L. E.; Menachery, V. D. Return of the Coronavirus: 2019-NCoV. *Viruses*. 2020. https://doi.org/10.3390/v12020135.

(6) Pillaiyar, T.; Manickam, M.; Namasivayam, V.; Hayashi, Y.; Jung, S. H. An Overview of Severe Acute Respiratory Syndrome-Coronavirus (SARS-CoV) 3CL Protease Inhibitors: Peptidomimetics and Small Molecule Chemotherapy. *Journal of Medicinal Chemistry*. 2016. https://doi.org/10.1021/acs.jmedchem.5b01461.

(7) Jin, Z.; Du, X.; Xu, Y.; Deng, Y.; Liu, M.; Zhao, Y.; Zhang, B.; Li, X.; Zhang, L.; Peng, C.; Duan, Y.; Yu, J.; Wang, L.; Yang, K.; Liu, F.; Jiang, R.; Yang, X.; You, T.; Liu, X.; Yang, X.; Bai, F.; Liu, H.; Liu, X.; Guddat, L. W.; Xu, W.; Xiao, G.; Qin, C.; Shi, Z.; Jiang, H.; Rao, Z.; Yang, H. Structure of M pro from COVID-19 Virus and Discovery of Its Inhibitors. https://doi.org/10.1038/s41586-020-2223-y.

(8) Anand, K.; Palm, G. J.; Mesters, J. R.; Siddell, S. G.; Ziebuhr, J.; Hilgenfeld, R. Structure of Coronavirus Main Proteinase Reveals Combination of a Chymotrypsin Fold with an Extra α-Helical Domain. *EMBO J.* **2002**, *21* (13). https://doi.org/10.1093/emboj/cdf327.

(9) Yang, H.; Yang, M.; Ding, Y.; Liu, Y.; Lou, Z.; Zhou, Z.; Sun, L.; Mo, L.; Ye, S.; Pang, H.; Gao, G. F.; Anand, K.; Bartlam, M.; Hilgenfeld, R.; Rao, Z. The Crystal Structures of Severe Acute Respiratory Syndrome Virus Main Protease and Its Complex with an Inhibitor. *Proc. Natl. Acad. Sci. U. S. A.* **2003**, *100* (23). https://doi.org/10.1073/pnas.1835675100.

(10) Chang, Y.; Tung, Y.; Lee, K.; Chen, T.; Hsiao, Y.; Chang, C.; Hsieh, T.; Su, C.; Wang, S.; Yu, J.; Lin, Y.; Lin, Y.; Tu, Y. E.; Tung, C. Potential Therapeutic Agents for COVID-19 Based on the Analysis of Protease and RNA Polymerase Docking. *Virol. J.* **2020**, No. February, 1–7. https://doi.org/10.20944/preprints202002.0242.v1.

(11) Procházková, D.; Boušová, I.; Wilhelmová, N. Antioxidant and Prooxidant Properties of Flavonoids. *Fitoterapia*. 2011. https://doi.org/10.1016/j.fitote.2011.01.018.
(12) Castañeda-Ovando, A.; Pacheco-Hernández, M. de L.; Páez-Hernández, M. E.; Rodríguez, J. A.; Galán-Vidal, C. A. Chemical Studies of Anthocyanins: A Review. *Food Chemistry*. 2009. https://doi.org/10.1016/j.foodchem.2008.09.001.
(13) Havsteen, B. H. The Biochemistry and Medical Significance of the Flavonoids. *Pharmacology and Therapeutics*. 2002. https://doi.org/10.1016/S0163-7258(02)00298-X.
(14) Parvez, M. K.; Tabish Rehman, M.; Alam, P.; Al-Dosari, M. S.; Alqasoumi, S. I.; Alajmi, M. F. Plant-Derived Antiviral Drugs as Novel Hepatitis B Virus Inhibitors: Cell Culture and Molecular Docking Study. *Saudi Pharm. J.* **2019**, *27* (3), 389–400. https://doi.org/10.1016/j.jsps.2018.12.008.
(15) Khan, M. S.; Bhat, S. A.; Rehman, M. T.; Hassan, I.; Tabrez, S.; AlAjmi, M. F.; Hussain, A.; Husain, F. M.; Alamery, S. F. Rutin Attenuates Negatively Charged Surfactant (SDS)-Induced Lysozyme Aggregation/Amyloid Formation and Its Cytotoxicity. *Int. J. Biol. Macromol.* **2018**, *120*, 45–58. https://doi.org/10.1016/j.ijbiomac.2018.07.112.
(16) Al-Shabib, N. A.; Khan, J. M.; Malik, A.; Alsenaidy, M. A.; Rehman, M. T.; AlAjmi, M. F.; Alsenaidy, A. M.; Husain, F. M.; Khan, R. H. Molecular Insight into Binding Behavior of Polyphenol (Rutin) with Beta Lactoglobulin: Spectroscopic, Molecular Docking and MD Simulation Studies. *J. Mol. Liq.* **2018**, *269*, 511–520. https://doi.org/10.1016/j.molliq.2018.07.122.
(17) Alajmi, M. F.; Alam, P.; Rehman, M. T.; Husain, F. M.; Khan, A. A.; Siddiqui, N. A.; Hussain, A.; Kalam, M. A.; Parvez, M. K. Interspecies Anticancer and Antimicrobial Activities of Genus Solanum and Estimation of Rutin by Validated UPLC-PDA Method. *Evidence-Based Complement. Altern. Med.* **2018**, *2018*, 1–13. https://doi.org/10.1155/2018/6040815.
(18) M. Calderon-Montano, J.; Burgos-Moron, E.; Perez-Guerrero, C.; Lopez-Lazaro, M. A Review on the Dietary Flavonoid Kaempferol. *Mini-Reviews Med. Chem.* **2011**, *11* (4). https://doi.org/10.2174/138955711795305335.
(19) Liu, R. H. Health-Promoting Components of Fruits and Vegetables in the Diet. *Adv. Nutr.* **2013**, *4* (3). https://doi.org/10.3945/an.112.003517.
(20) Kim, S. H.; Choi, K. C. Anti-Cancer Effect and Underlying Mechanism(s) of Kaempferol, a Phytoestrogen, on the Regulation of Apoptosis in Diverse Cancer Cell Models. *Toxicological Research*. 2013. https://doi.org/10.5487/TR.2013.29.4.229.
(21) Fang, F.; Huang, W.-D. Content of Potentially Anticarcinogenic Flavonoids of Tea Infusions, Wines, and Fruit Juices. *Eur. food Res. Technol.* **2013**, *237* (3). https://doi.org/10.1002/bies.950160209.
(22) Justesen, U.; Knuthsen, P. Composition of Flavonoids in Fresh Herbs and Calculation of Flavonoid Intake by Use of Herbs in Traditional Danish Dishes. *Food Chem.* **2001**, *73* (2). https://doi.org/10.1016/S0308-8146(01)00114-5.
(23) Stewart, A. J.; Bozonnet, S.; Mullen, W.; Jenkins, G. I.; Lean, M. E. J.; Crozier, A. Occurrence of Flavonols in Tomatoes and Tomato-Based Products. *J. Agric. Food Chem.* **2000**, *48* (7). https://doi.org/10.1021/jf000070p.
(24) Zheng, W.; Wang, S. Y. Antioxidant Activity and Phenolic Compounds in Selected Herbs. *J. Agric. Food Chem.* **2001**, *49* (11). https://doi.org/10.1021/jf010697n.
(25) Atanassova, M.; Bagdassarian, V. RUTIN CONTENT IN PLANT PRODUCTS. *J. Univ. Chem. Technol. Metall.* **2009**, *44* (2).
(26) Chang, S.; Tan, C.; Frankel, E. N.; Barrett, D. M. Low-Density Lipoprotein Antioxidant Activity of Phenolic Compounds and Polyphenol Oxidase Activity in Selected

Clingstone Peach Cultivars. *J. Agric. Food Chem.* **2000**, *48* (2). https://doi.org/10.1021/jf9904564.
(27) Malagutti, A. R.; Zuin, V. G.; Cavalheiro, É. T. G.; Mazo, L. H. Determination of Rutin in Green Tea Infusions Using Square-Wave Voltammetry with a Rigid Carbon-Polyurethane Composite Electrode. *Electroanalysis* **2006**, *18* (10). https://doi.org/10.1002/elan.200603496.
(28) Rehman, M. T.; Ahmed, S.; Khan, A. U. Interaction of Meropenem with 'N' and 'B' Isoforms of Human Serum Albumin: A Spectroscopic and Molecular Docking Study. *J. Biomol. Struct. Dyn.* **2016**, *34* (9), 1849–1864. https://doi.org/10.1080/07391102.2015.1094411.
(29) Rehman, M. T.; Dey, P.; Hassan, M. I.; Ahmad, F.; Batra, J. K. Functional Role of Glutamine 28 and Arginine 39 in Double Stranded RNA Cleavage by Human Pancreatic Ribonuclease. *PLoS One* **2011**, *6* (3), e17159. https://doi.org/10.1371/journal.pone.0017159.
(30) Morris, G. M.; Huey, R.; Lindstrom, W.; Sanner, M. F.; Belew, R. K.; Goodsell, D. S.; Olson, A. J. AutoDock4 and AutoDockTools4: Automated Docking with Selective Receptor Flexibility. *J. Comput. Chem.* **2009**, *30* (16), 2785–2791. https://doi.org/10.1002/jcc.21256.
(31) Rehman, M. T.; Shamsi, H.; Khan, A. U. Insight into the Binding Mechanism of Imipenem to Human Serum Albumin by Spectroscopic and Computational Approaches. *Mol. Pharm.* **2014**, *11* (6), 1785–1797. https://doi.org/10.1021/mp500116c.
(32) Hussain, A.; AlAjmi, M.; Rehman, M.; Khan, A.; Shaikh, P.; Khan, R. Evaluation of Transition Metal Complexes of Benzimidazole-Derived Scaffold as Promising Anticancer Chemotherapeutics. *Molecules* **2018**, *23* (5), 1232. https://doi.org/10.3390/molecules23051232.
(33) Rabbani, N.; Tabrez, S.; Islam, B. ul; Rehman, M. T.; Alsenaidy, A. M.; AlAjmi, M. F.; Khan, R. A.; Alsenaidy, M. A.; Khan, M. S. Characterization of Colchicine Binding with Normal and Glycated Albumin: In Vitro and Molecular Docking Analysis. *J. Biomol. Struct. Dyn.* **2018**, *36* (13), 3453–3462. https://doi.org/10.1080/07391102.2017.1389661.
(34) AlAjmi, M. F.; Rehman, M. T.; Hussain, A.; Rather, G. M. Pharmacoinformatics Approach for the Identification of Polo-like Kinase-1 Inhibitors from Natural Sources as Anti-Cancer Agents. *Int. J. Biol. Macromol.* **2018**, *116*, 173–181. https://doi.org/10.1016/j.ijbiomac.2018.05.023.
(35) Rehman, M.; AlAjmi, M.; Hussain, A.; Rather, G.; Khan, M. High-Throughput Virtual Screening, Molecular Dynamics Simulation, and Enzyme Kinetics Identified ZINC84525623 as a Potential Inhibitor of NDM-1. *Int. J. Mol. Sci.* **2019**, *20* (4), 819. https://doi.org/10.3390/ijms20040819.
(36) Amir, M.; Kumar, V.; Mohammad, T.; Dohare, R.; Rehman, M. T.; Alajmi, M. F.; Hussain, A.; Ahmad, F.; Hassan, M. I. Structural and Functional Impact of Non-Synonymous SNPs in the CST Complex Subunit TEN1: Structural Genomics Approach. December 27, 2018. https://doi.org/10.1101/507046.
(37) Brańka, A. C. Nosé-Hoover Chain Method for Nonequilibrium Molecular Dynamics Simulation. *Phys. Rev. E - Stat. Physics, Plasmas, Fluids, Relat. Interdiscip. Top.* **2000**, *61* (5), 4769–4773. https://doi.org/10.1103/PhysRevE.61.4769.
(38) Martyna, G. J.; Tobias, D. J.; Klein, M. L. Constant Pressure Molecular Dynamics Algorithms. *J. Chem. Phys.* **1994**, *101* (5), 4177–4189. https://doi.org/10.1063/1.467468.